Supporting Information for

All-in-One "Schizophrenic" Self-assembly of Orthogonally Tuned Thermo-responsive Diblock Copolymers

Natalya S. Vishnevetskaya,[†] Viet Hildebrand,[‡] Noverra M. Nizardo,[‡,$] Chia-Hsin Ko,[†] Zhenyu Di,[§] Aurel Radulescu,[§] Lester C. Barnsley,[§] Peter Müller-Buschbaum,[†,∥], André Laschewsky,[‡,⊥,], Christine M. Papadakis[†,*]*

[†]Fachgebiet Physik weicher Materie/Lehrstuhl für Funktionelle Materialien, Physik-Department, Technische Universität München, James-Franck-Straße 1, 85748 Garching, Germany

[‡]Institut für Chemie, Universität Potsdam, Karl-Liebknecht- Straße 24-25, 14476 Potsdam-Golm, Germany

[§]Forschungszentrum Jülich GmbH, Jülich Centre for Neutron Science at MLZ, Lichtenbergstr. 1, 85748 Garching, Germany

[∥]Heinz Maier-Leibnitz Zentrum (MLZ), Lichtenbergstr. 1, 85748 Garching, Germany

[⊥]Fraunhofer Institut für Angewandte Polymerforschung, Geiselbergstr. 69, 14476 Potsdam-Golm, Germany

[$]Permanent address N.M.N.: Department of Chemistry, University of Indonesia, Kampus UI Depok, Depok 16424, West-Java, Indonesia

14 pages, 4 figures and 5 tables.

Photographs of solutions

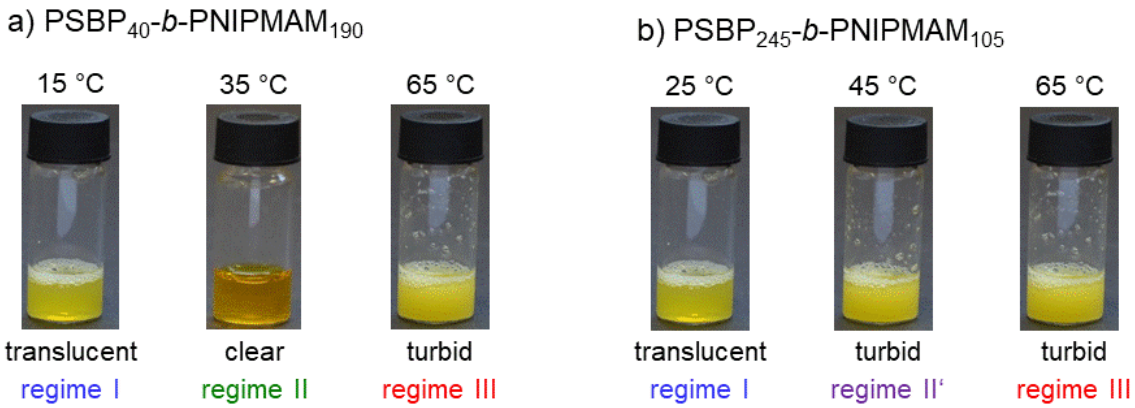

Figure S1. Photographs of 50 g L^{-1} solutions of (a) $PSBP_{40}$-*b*-$PNIPMAM_{190}$ in H_2O, showing a dissolved intermediate regime II, and of (b) $PSBP_{245}$-*b*-$PNIPMAM_{105}$, showing an insoluble intermediate regime II'.

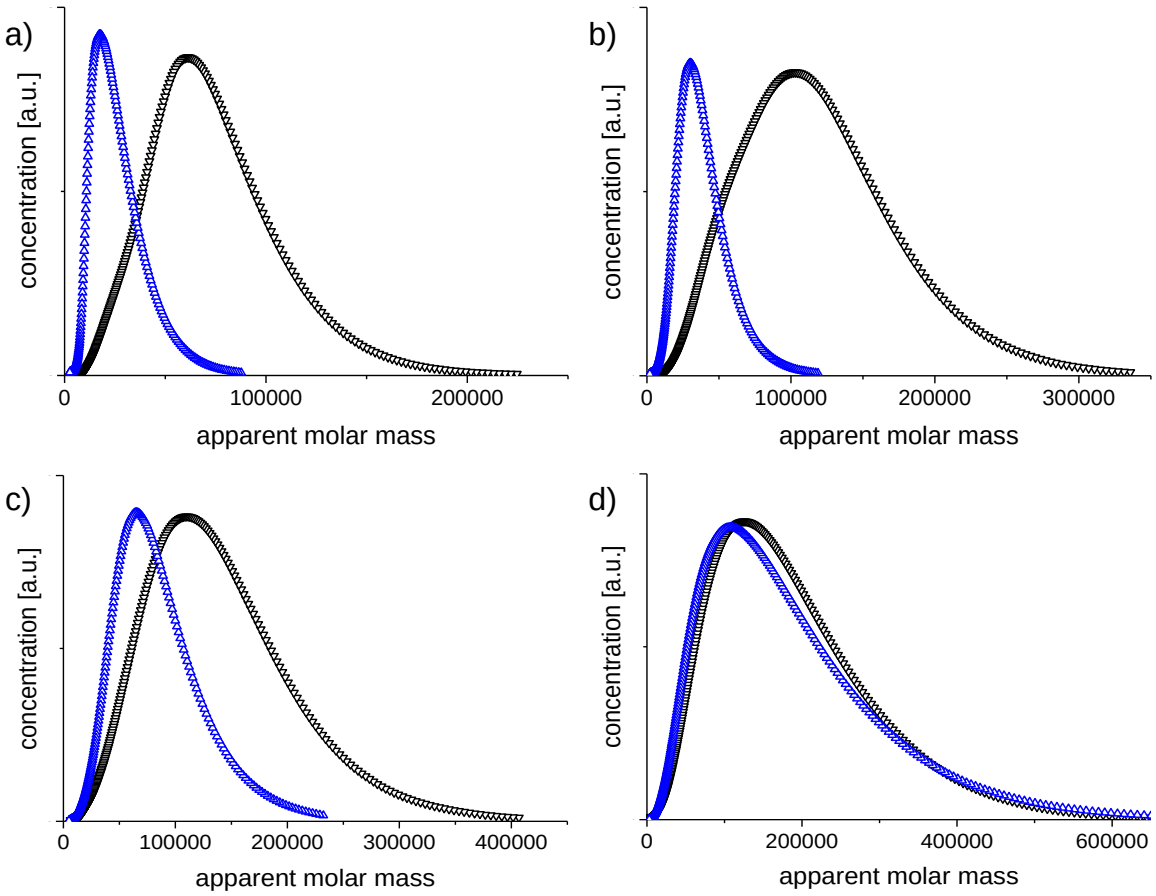

Figure S2. SEC elugrams of macro RAFT agents $PSBP_x$ (blue Δ), and of the derived block copolymers $PSBP_x$-*b*-$PNIPMAM_y$ (black ∇): (a) $PSBP_{40}$ and $PSBP_{40}$-*b*-$PNIPMAM_{190}$; (b) $PSBP_{50}$ and $PSBP_{50}$-*b*-$PNIPMAM_{155}$; (c) $PSBP_{245}$ and $PSBP_{245}$-*b*-$PNIPMAM_{105}$; (d) $PSBP_{425}$ and $PSBP_{425}$-*b*-$PNIPMAM_{110}$.

Conditions: eluent hexafluoroisopropanol (HFIP) containing 50 mM CF_3COONa, 40 °C, calibration with narrowly distributed poly(methyl methacrylate) standards 500 - 520,000 D.

Models used for fitting the SANS data

The SANS data were analyzed by fitting the following function:

$$I(q) = I_0 P(q) S(q) + I_{agg}(q) + I_{fluct}(q) + I_{bg} \quad \text{(S1)}$$

I_{bg} denotes the constant background, which was in all cases fixed at 0.45-0.6 cm^{-1}, I_0 a scaling factor and $P(q)$ the micellar form factor.

For $P(q)$, the form factor of polydisperse, homogeneous spheres was used with a Schulz distribution for the radii:[1]

$$P_{sphere}(q) = \left(\frac{4\pi}{3}\right)^2 N_0 (\Delta\rho)^2 \int_0^\infty f(r) r^6 F^2(q) dr \quad \text{(S2)}$$

where N_0 is the total number of particles per unit volume. $\Delta\rho$ is the difference in scattering length density of the sphere and the solvent: $\Delta\rho = \rho_{sphere} - \rho_{solvent}$ (values used see below). *f(r)* is the normalized Schulz distribution:[2]

$$f(r) = (z+1)^{z+1} u^z \frac{\exp[-(z+1)u]}{r_{avg}\Gamma(z+1)} \quad \text{(S3)}$$

$u = r/r_{avg}$, where r_{avg} denotes the average radius, $\Gamma(n)$ is the Gamma function, and z is related to the polydispersity p by $z = 1/(p^2-1)$: $p = \sigma/r_{avg}$, where σ^2 is the variance of the distribution. $F(q)$ is the scattering amplitude of a sphere having a radius r:

$$F(q) = \frac{3[\sin(qr) - qr\cos(qr)]}{(qr)^3} \quad \text{(S4)}$$

For the structure factor $S(q)$, we used the Percus-Yevick hard-sphere structure factor:[3]

$$S(q) = \frac{1}{1+24\eta G(2R_{HS}q)/2R_{HS}q} \quad \text{(S5)}$$

where R_{HS} is the hard-sphere radius, i.e. half the center-to-center distance between the particles. η is the hard sphere volume fraction, i.e. the fraction of micelles which are correlated, and

$$G(x) = \gamma \frac{\sin x - x\cos x}{x^2} + \delta \frac{2x\sin x + (2-x^2)\cos x - 2}{x^3} + \varepsilon \frac{-x^4\cos x + 4[3x^2 - 6\cos x + (x^3 - 6x)\sin x + 6]}{x^5} \quad \text{(S6)}$$

where $\gamma = (1+2\eta)^2/(1-\eta)^4$, $\delta = -6\eta(1+\eta/2)^2/(1-\eta)^4$ and $\varepsilon = \gamma\eta/2$.

For $PSBP_{50}$-*b*-$PNIPMAM_{155}$ at 40 °C and for $PSBP_{245}$-*b*-$PNIPMAM_{105}$ at 20-50 °C, no structure factor was necessary, and $S(q)$ was set to unity.

$I_{agg}(q)$ denotes the scattering from large aggregates. We used the Porod form factor:[4]

$$I_{agg}(q) = \frac{I_P}{q^\alpha} \quad \text{(S7)}$$

which comprises its amplitude I_P and the Porod exponent α. α is characteristic of the surface roughness of the aggregates: for particles with a smooth surface, $\alpha = 4$; for rough surfaces, $\alpha < 4$, and for a concentration gradient near the aggregate surface, $\alpha > 4$.[5] This term was not needed for $PSBP_{245}$-*b*-$PNIPMAM_{105}$ at 90 °C.

$I_{fluct}(q)$ describes concentration fluctuations. We used the Ornstein-Zernike term to model the scattering from concentration fluctuations in solutions of non-charged polymers:[6]

$$I_{OZ}(q) = \frac{I_{OZ}}{1+q^2\xi^2} \quad \text{(S8)}$$

which comprises an amplitude I_{OZ} and a correlation length, ξ_{OZ}. For $PSBP_{50}$-*b*-$PNIPMAM_{155}$ at 50-60 °C and for $PSBP_{245}$-*b*-$PNIPMAM_{105}$ in 24 mM NaBr in D_2O at 55 °C, instead of the Ornstein-Zernike term, the solvation term, $I_{solv}(q)$, was used:

$$I_{solv}(q) = CF_{solv}(q) \quad \text{(S9)}$$

The parameter *C* characterizes the solvation intensity, which reads:

$$C = A\frac{k_BT(\Delta\rho)^2}{K}, \quad \text{(S10)}$$

where *A* is a scaling factor related to the volume fraction, *K* is the osmotic compressibility, $(\Delta\rho)^2$ is the contrast factor with ρ being the scattering length densities of the polymers and the solvent, k_B is Boltzmann's constant and *T* the absolute temperature. $F_{solv}(x)$ is the scaling function, which is given by:

$$F_{solv}(q) = \frac{1}{1+(\lceil q-q_0\rceil\xi_{solv})^m}. \quad \text{(S11)}$$

$I_{solv}(q)$ was previously used to model concentration fluctuations in semidilute solutions of polyelectrolytes.[7] It features the parameter C characterizing the solvation intensity and the correlation length ξ_{solv}. The average distance $d_0 = 2\pi/q_o$ between the charged domains is calculated from the position of maximum intensity, q_0. For non-charged polymers, the solvation Porod exponent m is 5/3 in a good solvent or 2 in a theta solvent, respectively.[8]

The scattering length densities (SLD) of PSBP, PNIPMAM and D_2O were calculated at 7.3×10^{-5} nm^{-2}, 6.8×10^{-5} nm^{-2}, and 6.3×10^{-4} nm^{-2}, assuming mass densities of 1.0 g cm^{-3} for PSBP and 1.1 g cm^{-3} for PNIPMAM. In all fits of Eq. 1, the SLD values of the particles in regimes I and III were fixed at 7.1×10^{-5} nm^{-2}.

For the solution of $PSBP_{50}$-*b*-$PNIPMAM_{155}$ at 30 and 40 °C as well as the one of $PSBP_{245}$-*b*-$PNIPMAM_{105}$ at 40 °C, the curves were additionally modelled by:

$$I(q) = I_{agg}(q) + I_{solv}(q) + I_{bg} \quad \text{(S12)}$$

Modeling was performed using the SANS Data Reduction and Analysis software provided by the NIST Center for Neutron Research within the IGOR Pro software environment.[9]

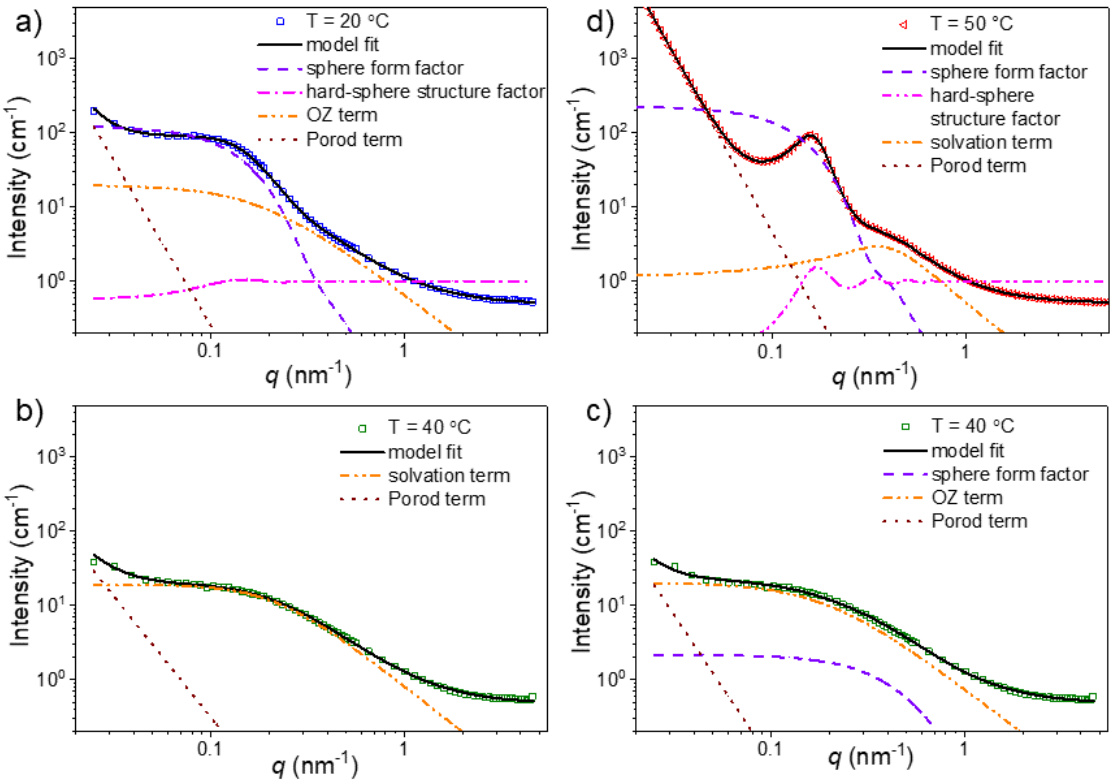

Figure S3. Details of model fitting to the SANS data of the 50 g L^{-1} $PSBP_{50}$-*b*-$PNIPMAM_{155}$ solution in salt-free D_2O in the 3 regimes (I: 20 °C, II: 40 °C, III: 50 °C), temperatures are given in the graphs. Symbols: data points, only every second point is shown. Full lines: Fits of Eq. 1 (a,c,d) and of Eq. 2(b). Broken lines: Contributions to the fits as described in the legends. OZ stands for Ornstein-Zernike.

Table S1. Best fit parameters of Eq. 1 for the SANS data of a 50 g L^{-1} $PSBP_{50}$-*b*-$PNIPMAM_{155}$ solution in salt-free D_2O in regimes I, II and III.

	Regime I		**Regime II**	**Regime III**	
	20 ºC	**30 ºC**	**40 ºC**	**50 ºC**	**60 ºC**
r_{avg} **[nm]**	11.1 ± 1.0	10.7 ± 1.1	1.7 ± 0.2	12.6 ± 0.1	12.9 ± 0.1
p	0.26 ± 0.03	0.23 ± 0.02	0.59 ± 0.05	0.20 ± 0.01	0.13 ± 0.01
R_{HS} **[nm]**	20 ± 2	19 ± 2		18.8 ± 0.1	17.9 ± 0.1
η	0.07 ± 0.01	0.08 ± 0.01		0.31 ± 0.02	0.32 ± 0.03
$I_P \times 10^9$	3.5 ± 0.3	0.6 ± 0.1	0.8 ± 0.1	1.8 ± 0.1	0.62 ± 0.01
α	4.4 ± 0.2	3.9 ± 0.2	3.6 ± 0.2	4.7 ± 0.1	4.9 ± 0.1
I_{OZ} **[cm^{-1}]**	20 ± 2	33 ± 3	20 ± 2		
ξ_{OZ} **[nm]**	5.4 ± 0.5	6.5 ± 0.6	5.1 ± 0.4		
C **[cm^{-1}]**				3.0 ± 0.1	0.9 ± 0.1
$\xi solv$ **[nm]**				3.8 ± 0.1	6.3 ± 0.1
m				1.7 ± 0.1	1.0 ± 0.1
d_0 **[nm]**				17.9 ± 0.3	11.1 ± 1
SLD sphere **[nm^{-2}]**	$(7.1 \pm 0.3) \times 10^{-5}$				

Table S2. Best fit parameters of Eq. 2 for the SANS data of a 50 g L^{-1} $PSBP_{50}$-*b*-$PNIPMAM_{155}$ solution in salt-free D_2O in regime I at 30 °C and regime II.

	Regime I **30 °C**	**Regime II** **40 ºC**
I_P	$(1.4 \pm 0.1) \times 10^{-8}$	$(9.7 \pm 0.8) \times 10^{-8}$
α	3.8 ± 0.2	3.3 ± 0.2
***C* [cm^{-1}]**	42 ± 4	19 ± 2
ξ_{solv} **[nm]**	9.9 ± 0.3	4.8 ± 0.2
m	1.82 ± 0.02	2.01 ± 0.02
d_0 **[nm]**	8 ± 1	15 ± 2

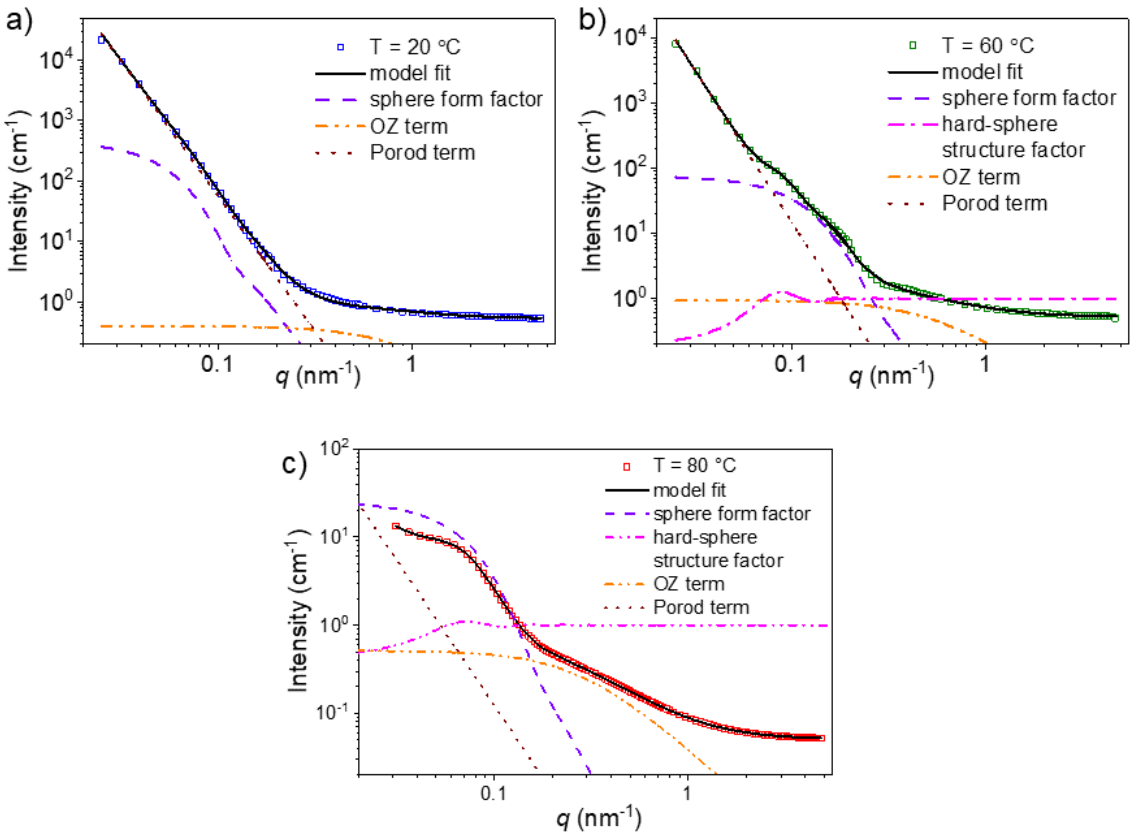

Figure S4. Details of model fitting to the SANS data of the 50 g L^{-1} $PSBP_{245}$-*b*-$PNIPMAM_{105}$ solution in salt-free D_2O in the 3 regimes (I: 20 °C, II': 60 °C, III: 80 °C), temperatures are given in the graphs. Symbols: data points, only every second point is shown. Full lines: Fits of Eq. 1. Broken lines: Contributions to the fits as described in the legends. OZ stands for Ornstein-Zernike.

Table S3. Best fit parameters of Eq. 1 for the SANS data of a 50 g L^{-1} $PSBP_{245}$-*b*-$PNIPMAM_{105}$ solution in salt-free D_2O.

	20 ºC	**30 ºC**	**40 ºC**	**50 ºC**	**60 ºC**	**60 ºC**	**70 ºC**	**80 ºC**	**90 ºC**
r_{avg} **[nm]**	32 ± 3	33 ± 3	42 ± 4	9 ± 1	13 ± 1	15 ± 1	19 ± 2	21 ± 2	12 ± 1
p	0.23 ± 0.02	0.23 ± 0.02	0.10 ± 0.01	0.26 ± 0.03	0.29 ± 0.03	0.25 ± 0.03	0.23 ± 0.03	0.27 ± 0.03	0.79 ± 0.08
R_{HS} **[nm]**					35 ± 3	37 ± 3	41 ± 4	41 ± 4	40 ± 4
η					0.22 ± 0.01	0.20 ± 0.02	0.19 ± 0.01	0.11 ± 0.01	0.15 ± 0.01
$I_P \times 10^8$	7.1 ± 0.6	6.2 ± 0.1	5.7 ± 0.5	3.2 ± 0.2	7.7 ± 0.7	14.1 ± 1.2	9.8 ± 0.9	3.5 ± 0.4	
α	4.5 ± 0.2	4.5 ± 0.2	4.5 ± 0.1	4.9 ± 0.3	4.6 ± 0.2	4.5 ± 0.2	3.6 ± 0.2	3.3 ± 0.2	
I_{OZ} **[cm^{-1}]**	0.4 ± 0.1	0.6 ± 0.1	0.8 ± 0.2	1.6 ± 0.3	0.9 ± 0.2	0.2 ± 0.2	0.3 ± 0.1	0.5 ± 0.1	0.6 ± 0.2
ξ_{OZ} **[nm]**	1.2 ± 0.1	1.5 ± 0.1	1.6 ± 0.1	2.6 ± 0.2	1.9 ± 0.2	2.1 ± 0.2	2.3 ± 0.2	3.5 ± 0.3	3.2 ± 0.3
SLD sphere **[nm^{-2}]**	$(7.1 \pm 0.3) \times 10^{-5}$								

Table S4. Best fit parameters of Eq. 1 for the SANS data of a 50 g L^{-1} $PSBP_{245}$-*b*-$PNIPMAM_{105}$ solution in 24 mM NaBr in D_2O.

	20 ºC	**55 ºC**
r_{avg} **[nm]**	22.7 ± 0.1	23.92 ± 0.05
p	0.303 ± 0.004	0.224 ± 0.002
R_{HS} **[nm]**		31.06 ±0.04
η		0.255 ± 0.001
$I_P \times 10^{11}$	4.03 ± 0.06	112.7 ± 0.4
α	5.20 ± 0.03	4.5
I_{OZ} **[cm^{-1}]**	2.08 ± 0.02	
ξ_{OZ} **[nm]**	4.7 ± 0.3	
C **[cm^{-1}]**		1.26 ± 0.01
$\xi solv$ **[nm]**		4.30 ±0.03
m		1.91 ±0.01
d_0 **[nm]**		32.3 ±0.5
SLD sphere **[nm^{-2}]**	7.1×10^{-5}	

Table S5. Best fit parameters of Eq. 2 for the SANS data of a 50 g L^{-1} $PSBP_{245}$-*b*-$PNIPMAM_{105}$ solution in 24 mM NaBr in D_2O in regime II at 40 °C.

	Regime II **40 ºC**
C **[cm^{-1}]**	5.38 ± 0.02
ξ_{solv} **[nm]**	4.78 ± 0.01
m	2.406 ± 0.003
d_0 **[nm]**	

(1) Kotlarchyk, M.; Chen, S-H. Analysis of Small Angle Neutron Scattering Spectra from Polydisperse Interacting Colloids. *J. Chem. Phys.* **1983**, *79*, 2461-2469.

(2) Schulz, G. V. Über die Kinetik der Kettenpolymerisationen. *Z. Phys. Chem.* **1935**, *43*, 25-46.

(3) Percus, J. K.; Yevick, G. Analysis of Classical Statistical Mechanics by Means of Collective Coordinates. *J. Phys. Rev.* **1958**, *110*, 1-13.

(4) Porod, G. Die Röntgenkleinwinkelstreuung von dicht gepackten kolloiden Systemen. *Kolloid-Z.* **1951**, *123*, 83-114.

(5) Koberstein, J. T.; Morra, B.; Stein, R. S. The Determination of Diffuse-Boundary Thicknesses of Polymers by Small-Angle X-ray Scattering. *J. Appl. Crystallogr.* **1980**, *13*, 34−45.

(6) Shibayama, M.; Tanaka, T. Small Angle Neutron Scattering Study on Poly(N-isopropyl acrylamide) Gels Near their Volume-Phase Transition Temperature. *J. Chem. Phys.* **1992**, *97*, 6829-6841.

(7) Horkay, F.; Hammouda, B. Small-angle Neutron Scattering from Typical Synthetic and Biopolymer Solutions. *Colloid Polym. Sci.* **2008**, *286*, 611−620.

(8) Feuz, L.; Strunz, P.; Geue, T.; Textor, M.; Borisov, O. Conformation of Poly(L-lysine)-graft-poly(ethylene glycol) Molecular Brushes in Aqueous Solution Studied by Small-Angle Neutron Scattering. *Eur. Phys. J.* **2007**, *23*, 237–245.

(9) Kline, S. R. Reduction and Analysis of SANS and USANS Data Using IGOR Pro. *J. Appl. Crystallogr*. **2006**, *39*, 895.